

USE OF AN ACTIVE ELECTRO-HYDROSTATIC ACTUATION SYSTEM FOR VEHICLE VIBRATION DAMPING APPLICATIONS

Andrea Tonoli¹, Nicola Amati¹, Renato Galluzzi*¹, Francesco Fornari*²

¹Politecnico di Torino - Turin, Italy
{andrea.tonoli,nicola.amati,renato.galluzzi}@polito.it

²AMET s.r.l. - Turin, Italy
francesco.fornari@amet.it

Keywords: electro-hydrostatic actuation, active shock absorber, vehicle suspension.

Abstract. *Conventional vibration damping in wheeled vehicles is mainly performed by means of passive hydraulic systems. Active and semi-active solutions are adopted when there is particular interest in varying the damping response of the shock absorbers for vehicle handling and comfort. To this end, electro-hydrostatic actuation (EHA) devices represent a promising alternative in active vibration control. In these systems, an electric motor is employed to drive a fixed-displacement hydraulic pump. The flow generated by the pump is then conducted into a hydraulic piston that acts as a conventional damper. The use of a motor as a primary actuation device eases the control task and offers a large output bandwidth. This feature represents an advantage with respect to active hydraulic technologies, which attain limited bandwidth frequencies and use highly nonlinear servo-valves. Moreover, the reversible nature of the electric machine in EHA actuators allows part of the energy exchanged during damping to be recovered. When compared to electromechanical shock absorbers, EHA devices offer higher output power densities and higher efficiencies. In this context, the present paper describes the design, modelling and control of an active EHA system utilized for vehicle damping purposes. An overview of the current active solutions and a comparison with the EHA technology are revised. Results in terms of damping response and energy harvesting capabilities are then discussed.*

1 INTRODUCTION

Road roughness is the main source of vibrations for a wheeled vehicle [1], inevitably penalizing ride comfort, road-holding and, in general, vehicle performance. Suspension systems attenuate these effects on the car body and the tyre by utilizing elastic and damping devices. The classic suspension employs purely mechanical elements, i.e. coil springs and passive hydraulic dampers, that are suitably interfaced to the vehicle chassis. This entire system provides a fixed dynamic behaviour mainly related to the stiffness of the spring and the tyre, the viscous friction of the damper and the sprung and unsprung masses.

However, there is an increasing interest in controlling the damping properties of the suspension, aiming to improve performance on a vast diversity of terrain profiles. The possible solutions can be classified into two main categories, according to their energy consumption [2]:

- *Active suspensions*, if there is an energy exchange between the suspension elements and the vehicle.
- *Semi-active suspensions*, when the energy consumption is limited to drive the suspension actuators, without taking part of the actual damping response.

Generally speaking, active devices present a higher degree of flexibility when compared to semi-active ones, since can provide or absorb energy according to the road conditions and desired response. This reversibility is achieved using an electric motor with a suitable transmission system.

The choice of a mechanism that opportunely interfaces the electric motor to the output of the damper is not trivial. Moreover, the complexity increases when transforming rotation into translation motion, which is a choice constrained by the need of output power densities not achievable with linear motors. The work presented in [3] introduces an outline of possible configurations for the particular case of electromechanical shock absorbers (EMSA). However, aspects such as complexity, costliness, bulkiness and tribology issues are non-negligible drawbacks of these actuators.

The present paper addresses the use of an electro-hydrostatic actuator (EHA) as an active damping system for vehicle vibration control. The main objective of this work is to present a simple, compact and energy-efficient solution that is capable of delivering the required damping response for small and medium-size vehicles. For this purpose, the layout and the model of the actuator are introduced. A simple control algorithm is then implemented to test the capabilities of the device and results in the frequency and time domains are carried out and discussed.

2 SYSTEM LAYOUT

The EHA system shown in Figure 1 consists of a hydraulic actuator driven by an external gear pump by means of two pipelines. This pump is also coupled to an electric motor. In this way, the linear motion of the piston produces a fluid flow in the hydraulic circuit, thus inducing a rotational displacement in the pump and motor shafts. The electric machine can be controlled to yield a desired output torque that is transformed into a damping force by means of the same principle.

It is worth noting that power can flow either from the suspension to the motor or vice versa. This bidirectionality allows integrating the system in a active suspension. A similar configuration is implemented in [4]. In that case, however, the power delivered by the motor is used only to exert active forces, while the damping task is accomplished by two variable-orifice valves.

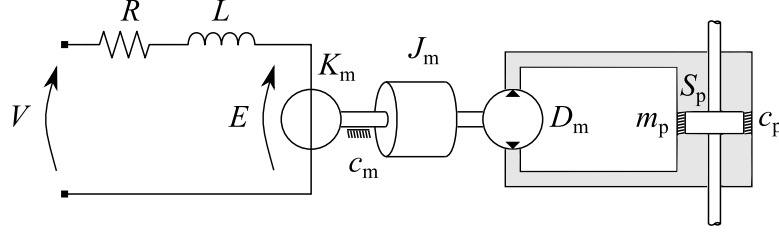


Figure 1: EHA System layout

The given representation integrates a DC electric motor with winding resistance R , inductance L and constant K_m , although a generalization to other types of motors such as brushless permanent-magnet machines can be performed as well. The coupling between the shafts of the motor and the pump is assumed ideally rigid. The viscous friction and moment of inertia of both components can be lumped into single parameters c_m and J_m , respectively. In the hydraulic domain, the pump is assumed to have a displacement D_m and unitary volumetric efficiency. Both pipelines are symmetric and an ideally-stiff fluid inside them is assumed for the bandwidth of interest. This simplification is possible for a well-filled hydraulic circuit with a small volume of oil, since the hydraulic stiffness is given by

$$k_{\text{hyd}} = \frac{\beta_{\text{oil}}}{V_{\text{oil}}}, \quad (1)$$

where β_{oil} is the bulk modulus of the oil and V_{oil} is its volume. Furthermore, the inertia of the fluid is calculated as

$$I_{\text{hyd}} = \rho_{\text{oil}} \frac{l}{A}, \quad (2)$$

where ρ_{oil} is the oil density, l the length of the pipelines and A their cross section. Assuming short pipelines, this term can also be neglected. The conversion of power from the hydraulic to the mechanical domain is performed by a piston of constant surface S_p , mass m_p and viscous damping coefficient c_p . Temperature effects are neglected in all the components of the model.

2.1 Dynamic Model

The quarter-car model shown in Figure 2a is used to evaluate the vehicle vertical dynamics when driving through a terrain profile denoted by the time function h ¹. The sprung mass m_s represents the vehicle chassis and the unsprung mass m_u takes into account the suspension structure inertia. The suspension stiffness and damping are expressed by k_s and c_s , respectively. The tyre stiffness is lumped by k_u . The dynamics of each mass are defined by the generalized coordinates x_i .

Taking into account the previously stated assumptions, the EHA damper can be integrated into the quarter-car model as a substitute of the viscous damper c_s , thus yielding the model in Figure 2b. The EHA actuator has an equivalent mass and an equivalent viscous damping:

$$m_{\text{eq}} = m_p + \frac{J_m}{r^2}, \quad (3)$$

$$c_{\text{eq}} = c_p + \frac{c_m}{r^2}, \quad (4)$$

¹The time dependence was omitted in all the functions for notation simplicity.

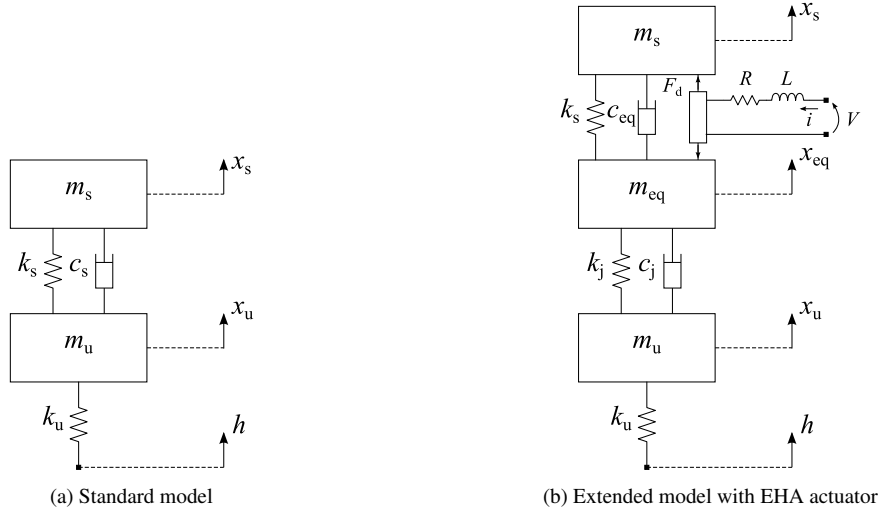


Figure 2: Quarter-car models

where

$$\tau = \frac{D}{S_p} \quad (5)$$

is the transmission ratio of the actuator. An additional stiffness-viscous damping couple (k_j , c_j) is introduced to model the mount that links the damper to the suspension structure. Its inclusion in the standard quarter-car model is irrelevant as the viscous damper c_s is assumed to be massless. Since the equivalent mass of the EHA actuator is non-negligible, the joint compliance has an important contribution to the frequency response of the system.

The electrical domain presents a linear gyrator that produces an output force proportional to the current in its windings:

$$F_d = \frac{K_m}{\tau} i. \quad (6)$$

The circuit behaviour is defined by the differential equation

$$L \frac{di}{dt} + Ri + \frac{K_m}{\tau} v_d = V, \quad (7)$$

where a voltage V is used to drive a device that produces an electromotive force (emf) proportional to its stroke speed v_d .

The mechanical domain can be defined by three differential equations:

$$m_s \ddot{x}_s + c_{eq}(\dot{x}_s - \dot{x}_{eq}) + k_s(x_s - x_{eq}) = F_d, \quad (8)$$

$$m_{eq} \ddot{x}_{eq} + c_{eq}(\dot{x}_{eq} - \dot{x}_s) + c_j(\dot{x}_{eq} - \dot{x}_u) + k_s(x_{eq} - x_s) + k_j(x_{eq} - x_u) = -F_d; \quad (9)$$

$$m_u \ddot{x}_u + c_j(\dot{x}_u - \dot{x}_{eq}) + k_j(x_u - x_{eq}) + k_u(x_u - h) = 0. \quad (10)$$

A state-space representation of the extended quarter-car model can be obtained by substituting Equation 7 into Equations 8 and 9 and assuming

$$v_d = \dot{x}_s - \dot{x}_{eq}. \quad (11)$$

$$\dot{\mathbf{x}}_e = \mathbf{A}_e \mathbf{x}_e + \mathbf{B}_e \mathbf{u}_e \quad (12)$$

$$\mathbf{y}_e = \mathbf{C}_e \mathbf{x}_e \quad (13)$$

$$\mathbf{x}_e^\top = [x_s \quad x_{eq} \quad x_u \quad \dot{x}_s \quad \dot{x}_{eq} \quad \dot{x}_u \quad i] \quad (14)$$

$$\mathbf{u}_e^\top = [h \quad V] \quad (15)$$

$$\mathbf{y}_e^\top = [v_d \quad \ddot{x}_s \quad i] \quad (16)$$

$$\mathbf{A}_e = \begin{bmatrix} 0 & 0 & 0 & 1 & 0 & 0 & 0 & 0 \\ 0 & 0 & 0 & 0 & 1 & 0 & 0 & 0 \\ 0 & 0 & 0 & 0 & 0 & 1 & 0 & 0 \\ -\frac{k_s}{m_s} & \frac{k_s}{m_s} & 0 & -\frac{c_{eq}}{m_s} & \frac{c_{eq}}{m_s} & 0 & \frac{K_m}{\tau m_s} & 0 \\ \frac{k_s}{m_{eq}} & -\frac{k_s+k_j}{m_{eq}} & \frac{k_j}{m_{eq}} & \frac{c_{eq}}{m_{eq}} & -\frac{c_{eq}+c_j}{m_{eq}} & \frac{c_j}{m_{eq}} & -\frac{K_m}{\tau m_{eq}} & 0 \\ 0 & \frac{k_j}{m_u} & -\frac{k_j+k_u}{m_u} & 0 & \frac{c_j}{m_u} & -\frac{c_j}{m_u} & 0 & 0 \\ 0 & 0 & 0 & -\frac{K_m}{\tau L} & \frac{K_m}{\tau L} & 0 & 0 & -\frac{R}{L} \end{bmatrix} \quad (17)$$

$$\mathbf{B}_e^\top = \begin{bmatrix} 0 & 0 & 0 & 0 & 0 & 0 & \frac{1}{L} & 0 \\ 0 & 0 & 0 & 0 & 0 & \frac{k_u}{m_u} & 0 & 0 \end{bmatrix} \quad (18)$$

$$\mathbf{C}_e = \begin{bmatrix} 0 & 0 & 0 & 1 & -1 & 0 & 0 & 0 \\ -\frac{k_s}{m_s} & \frac{k_s}{m_s} & 0 & -\frac{c_{eq}}{m_s} & \frac{c_{eq}}{m_s} & 0 & \frac{K_m}{\tau m_s} & 0 \\ 0 & 0 & 0 & 0 & 0 & 0 & 0 & 1 \end{bmatrix} \quad (19)$$

In a similar fashion, a state-space form can be deduced for the standard model (Figure 2a).

$$\dot{\mathbf{x}}_q = \mathbf{A}_q \mathbf{x}_q + \mathbf{B}_q \mathbf{u}_q \quad (20)$$

$$\mathbf{y}_q = \mathbf{C}_q \mathbf{x}_q \quad (21)$$

$$\mathbf{x}_q^\top = [x_s \quad x_u \quad \dot{x}_s \quad \dot{x}_u] \quad (22)$$

$$\mathbf{u}_q = h \quad (23)$$

$$\mathbf{y}_q = \ddot{x}_s \quad (24)$$

$$\mathbf{A}_q = \begin{bmatrix} 0 & 0 & 1 & 0 \\ 0 & 0 & 0 & 1 \\ -\frac{k_s}{m_s} & \frac{k_s}{m_s} & -\frac{c_s}{m_s} & \frac{c_s}{m_s} \\ \frac{k_s}{m_u} & -\frac{k_s+k_u}{m_u} & \frac{c_s}{m_u} & -\frac{c_s}{m_u} \end{bmatrix} \quad (25)$$

$$\mathbf{B}_q^\top = [0 \quad 0 \quad 0 \quad \frac{k_u}{m_u}] \quad (26)$$

$$\mathbf{C}_q = [-\frac{k_s}{m_s} \quad \frac{k_s}{m_s} \quad -\frac{c_s}{m_s} \quad \frac{c_s}{m_s}] \quad (27)$$

3 CONTROL STRATEGY

3.1 Control Loop

The EHA actuator can be controlled within a feedback loop to obtain a desired damping behaviour. To this end, the layout presented in Figure 3 is introduced for the extended quarter-car model. It contains a transfer function matrix

$$\mathbf{G}_e = \mathbf{C}_e (s\mathbf{I} - \mathbf{A}_e)^{-1} \mathbf{B}_e = \begin{bmatrix} \frac{\ddot{x}_s}{h} & \frac{\ddot{x}_s}{V} \\ \frac{v_d}{h} & \frac{v_d}{V} \\ \frac{i}{h} & \frac{i}{V} \end{bmatrix} = \begin{bmatrix} G_x^h & G_x^V \\ G_v^h & G_v^V \\ G_i^h & G_i^V \end{bmatrix}, \quad (28)$$

which provides all the plant input-output mappings in the Laplace domain. The stroke speed v_d is calculated from the measurements of a rotary position sensor and preprocessed by G_r to yield a current reference. The gyrotor current is then measured and compared with the reference to compute the current error. A compensator G_c calculates the command from this signal to drive the power stage G_a that feeds a voltage into the actuator.

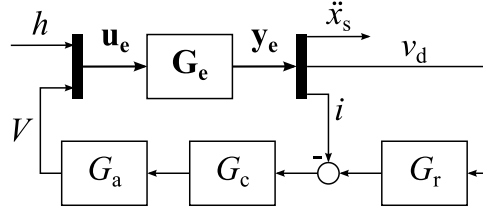


Figure 3: Control loop

At this point, the frequency response of the transfer function between the sprung mass acceleration and the road profile ($\ddot{x}_s(j\omega)/h(j\omega)$) is calculated for both the extended and the standard quarter-car models. A subsequent comparison will be carried out in the next section.

$$F_e(j\omega) = \left[G_x^h + G_x^v G_a G_c \left(\frac{G_r G_v^h - G_i^h}{1 + G_i^v G_a G_c - G_v^v G_a G_c G_r} \right) \right]_{s=j\omega} \quad (29)$$

$$F_q(j\omega) = \mathbf{C}_q (s\mathbf{I} - \mathbf{A}_q)^{-1} \mathbf{B}_q \quad (30)$$

The control-loop blocks G_r , G_c and G_a are defined according to the desired output damping. In particular, the sprung-mass viscous damping was chosen by using

$$c_s = \sqrt{\frac{k_s(m_s + m_u)}{2}} \sqrt{\frac{k_u + 2k_s}{k_u}}. \quad (31)$$

This value can be found by trying to keep the sprung mass acceleration as low as possible in a large range of frequencies [5]. Following this choice, the current reference is generated by a simple gain block, where

$$G_r = -\frac{\tau}{K_m} c_s. \quad (32)$$

Furthermore, the compensator is a simple proportional integral controller

$$G_c = K_P + \frac{K_I}{s} \quad (33)$$

and the actuator is modelled with a gain and a first-order delay approximation related to the switching frequency of the power module:

$$G_a = \frac{V_{DC}}{1 + \frac{sT_{sw}}{2}} \quad (34)$$

3.2 Driving Set-Up

The power module that feeds the motor consists of a full H-bridge connected to a capacitor-stabilized battery. The battery recharging circuit is neglected for simplicity. The implemented driving strategy is based on the work presented in [6] due to its advantages in terms of cost and

efficiency. Figure 4 introduces two switching phases. During phase A, a current is induced on the windings of the gyrator by imposing its own back emf and the battery voltage to the armature. This is a power-consuming braking operation that requires two closed switches. Phase B, on the other hand, lets the current flow through the free-wheeling diodes back to the battery to decrease the braking intensity. Such condition is power-regenerative. Both conditions are alternated at high frequency to produce a controlled mean-damping response.

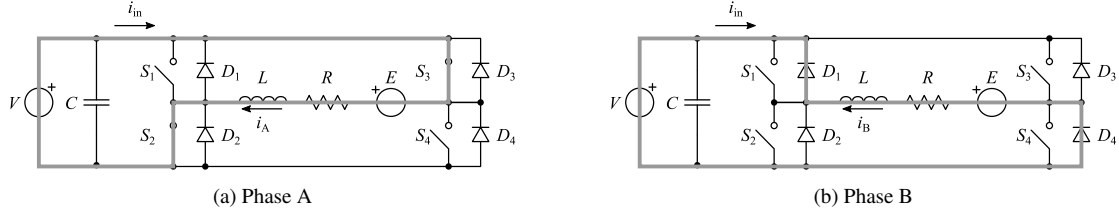


Figure 4: Driving phases

Applying the same sequence to opposed switching devices (for example, S_1 and S_4 instead of S_2 and S_3) yields a controlled motor torque. In this way, the driving strategy spans the four operating quadrants of the actuator, which is a necessary condition for full-active suspensions.

4 RESULTS

Considering the models developed in the previous sections, Table 1 lists the parameters employed to test the suspension capabilities.

Symbol	Description	Value	Unit
m_s	Sprung mass	250	kg
m_u	Unsprung mass	25	kg
c_s	Sprung mass viscous damping	2.27×10^3	Ns/m
k_s	Sprung mass stiffness	25×10^3	N/m
k_u	Unsprung mass stiffness	1×10^5	N/m
c_j	Mount viscous damping	4×10^3	Ns/m
k_j	Mount stiffness	4×10^6	N/m
J_m	Motor-pump moment of inertia	4×10^{-5}	kgm ²
m_p	Piston mass	0.67	kg
D_m	Pump displacement	1.8	cm ³ /rev
S_p	Piston surface	1.76	cm ²
K_m	Motor constant	0.11	Nm/A
R	Motor winding resistance	0.7	Ω
L	Motor winding inductance	0.677	mH
f_{sw}	Power module switching frequency	12	kHz

Table 1: Simulation parameters for standard and extended quarter-car models

4.1 Frequency-Domain Simulations

Figure 5 shows a comparison between the extended and standard models in a magnitude Bode plot. Figure 6 illustrates the parametric sensitivity of $|F_e(j\omega)|$ with respect to the equiva-

lent mass and the joint stiffness, respectively.

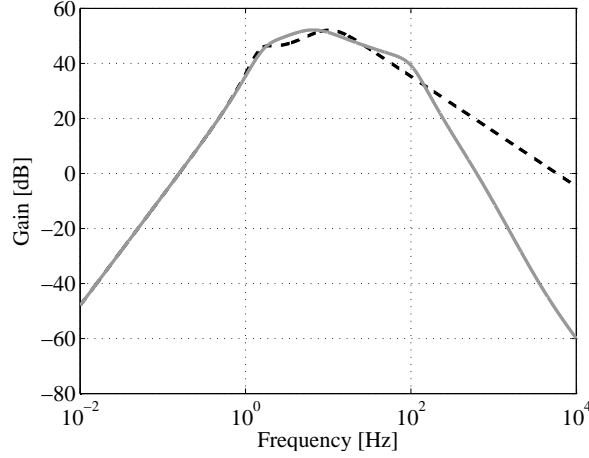


Figure 5: Magnitude of the frequency response, extended model (F_e , solid line) and standard model (F_q , dashed line)

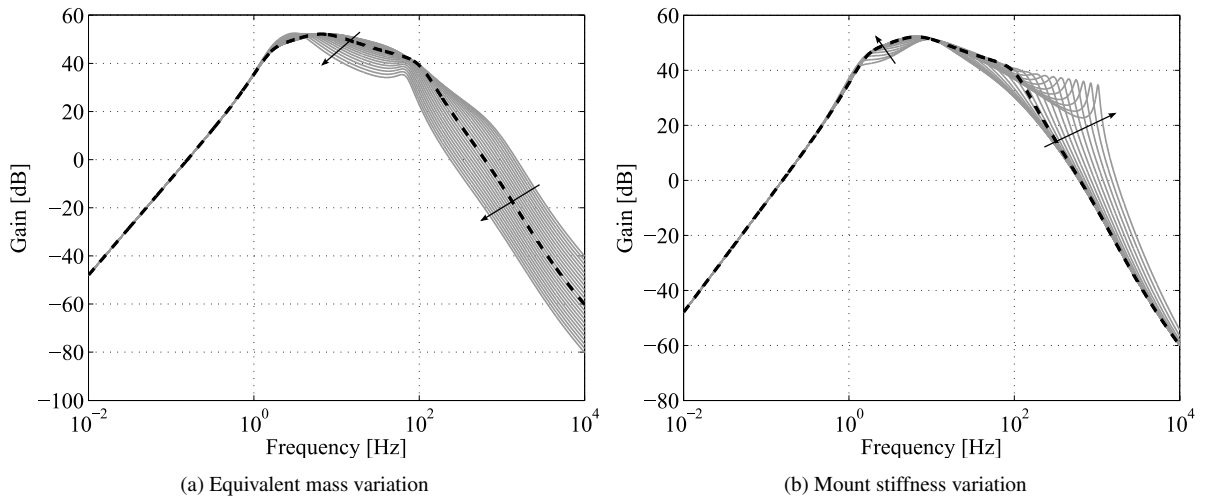


Figure 6: Parametric sensitivity of the extended model $|F_e(j\omega)|$. The arrows indicate the behaviour trend of the different responses (solid lines) with respect to the nominal condition (dashed line) as the respective parameters increase.

The standard model response presents two resonant peaks due to the sprung mass and unsprung mass natural frequencies. Besides these peaks, the extended model presents also a third frequency related to the equivalent mass that is not possible to observe since the three natural frequencies together produce a smooth response between 4 and 80 Hz. A parametric variation of m_{eq} shows that the resonant peak of the equivalent mass decreases in frequency and may produce a low-frequency sharp peak. By converse, a lower equivalent mass will induce higher amplification at higher frequencies (100 Hz). Considering human comfort as one of the main targets in suspension design, it is preferable to tune the equivalent mass as low as possible to avoid unwanted oscillations at low frequencies (SAE ride frequency range). This choice depends on the selection of an adequate reduction ratio that depends on the trade-off between compactness and low equivalent mass. Furthermore, the mount stiffness parametric

study suggests the use of materials with a certain degree of compliance to prevent high frequency resonances.

In general, a good agreement between the nominal and extended models is found up to $\omega_p = R/L$, the electric pole natural frequency of the motor, which imposes a limit to the dynamic damping capability of the device.

4.2 Time-Domain Simulations

Figure 7 shows a simulation of the sprung mass acceleration while driving on a generic off-road terrain profile. The acceleration of the sprung mass of both models is practically identical. A plot of the power consumption shows that phase A and B are practically equal, thus the consumed power during phase A is completely regenerated by phase B.

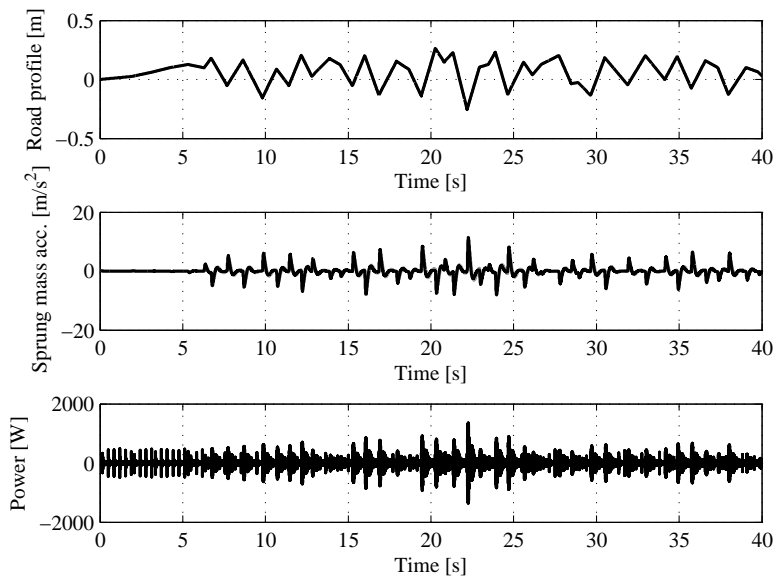


Figure 7: Time-domain results. The sprung mass acceleration is measured on both systems (black: extended model, grey: standard model). The power consumption is indicated by a positive sign.

5 CONCLUSIONS

The present paper introduced a simple and energy-efficient layout. Details of modelling and a validation using a simple control strategy were discussed. The proposed actuator is capable of delivering the required damping performance for a mid-size vehicle. The importance of an adequate selection of the equivalent mass and the mount stiffness were remarked. Further developments of this work include the test of a real EHA prototype for validation purposes.

REFERENCES

- [1] J. Y. Wong, *Theory of ground vehicles, 3rd edition*, John Wiley & Sons Inc., New York, 2001.
- [2] M. Savaresi *et al.*, *Semi-active suspension control design for vehicles*, Butterworth-Heinemann, Kidlington, UK, 2010.
- [3] A. Tonoli , N. Amati , J. G. Detoni , R. Galluzzi and E. Gasparin, *Modelling and validation of electromechanical shock absorbers*, *Vehicle System Dynamics: International Journal of Vehicle Mechanics and Mobility*, DOI:10.1080/00423114.2013.789538, 2013.
- [4] O. Ajala, D. Bestle, J. Rauh, *Modelling and control of an electro-hydraulic active suspension system*, *Archive of Mechanical Engineering*. Volume LX, Issue 1, Pages 3754, ISSN (Print) 0004-0738, DOI: 10.2478/meceng-2013-0003, March 2013.
- [5] G. Genta and L. Morello, *The Automotive Chassis: Volume 2: System Design (Mechanical Engineering Series)*, Springer, 2009.
- [6] M. Yang, H. Zhou, B. Ma, K. Shyu, *A cost-effective method of electric brake with energy regeneration for electric vehicles*, *IEEE Transactions on Industrial Electronics*, Vol. 56, No. 6, June 2009, pp. 2203-2212.